nature materials

ARTICLES

PUBLISHED ONLINE: 19 JUNE 2017 | DOI: 10.1038/NMAT4919

Universal quinone electrodes for long cycle life aqueous rechargeable batteries

Yanliang Liang[1], Yan Jing[1], Saman Gheytani[1], Kuan-Yi Lee[1], Ping Liu[2], Antonio Facchetti[3]* and Yan Yao[1,4]*

Aqueous rechargeable batteries provide the safety, robustness, affordability, and environmental friendliness necessary for grid storage and electric vehicle operations, but their adoption is plagued by poor cycle life due to the structural and chemical instability of the anode materials. Here we report quinones as stable anode materials by exploiting their structurally stable ion-coordination charge storage mechanism and chemical inertness towards aqueous electrolytes. Upon rational selection/design of quinone structures, we demonstrate three systems that coupled with industrially established cathodes and electrolytes exhibit long cycle life (up to 3,000 cycles/3,500 h), fast kinetics (≥20C), high anode specific capacity (up to 200–395 mAh g^{-1}), and several examples of state-of-the-art specific energy/energy density (up to 76–92 Wh kg^{-1}/ 161–208 Wh l^{-1}) for several operational pH values (−1 to 15), charge carrier species (H^+, Li^+, Na^+, K^+, Mg^{2+}), temperature (−35 to 25 °C), and atmosphere (with/without O_2), making them a universal anode approach for any aqueous battery technology.

The increasing demand for integration of electricity generated from renewable energies into the grid and electrification of transportation vehicles call for batteries that are environmentally friendly, safe, inexpensive, and long lasting[1,2]. Aqueous rechargeable batteries[3–6] featuring low-cost and nonflammable water-based electrolytes are intrinsically safe and do not rely heavily on the protection from complex battery management systems, thereby providing robustness and cost advantages over competing lithium-ion batteries that use volatile organic electrolytes and are responsible for recent catastrophic explosions. However, state-of-the-art aqueous rechargeable batteries show short cycle life[7] and fall short of meeting large-scale applications where frequent replacement of batteries is undesirable.

The anode materials have been the cycle-life-limiting component for most, if not all, aqueous rechargeable batteries[8–10]. For example, lead-based acidic batteries are inexpensive and reliable but have poor cycle life (200 cycles for deep cycling[7]) due to the premature ageing of the lead (Pb) anode into a thick $PbSO_4$ passivation layer[8]. No other faradaic electrode material has been discovered to work as anode for acid batteries. Recent efforts to substitute Pb with non-faradaic activated carbon (AC) extend cycle life at the cost of ~60% reduction in specific energy[11–13]. Another established family of aqueous rechargeable batteries are nickel-based alkaline batteries, including nickel–iron, nickel–cadmium, nickel–zinc, and nickel–metal hydride (MmH) batteries, which consist of the same nickel hydroxide ($Ni(OH)_2$) cathode but varying anodes[10,14]. However, iron, cadmium, and zinc anodes undergo dissolution–precipitation, while MmH volume expansion–contraction during battery charge–discharge cycling negatively impacts cycle life. The comparatively most stable MmH is made of rare earth metals and the expensive cobalt, with the latter accounting for one-half of the total material cost for a nickel–MmH battery[15]. The emerging aqueous lithium-ion batteries (ALIBs) use less corrosive, near-neutral electrolytes and store charge via an ion intercalation mechanism where the structure of the electrode material does not alter significantly[16–19]. Therefore, ALIBs could achieve a much longer cycle life than those of their commercial acidic and alkaline siblings. However, the only two practical anodes for ALIBs, lithium metal phosphates[9,20] and polyimides[21,22], are unstable to oxygen and alkalis, respectively, severely restricting applications. Finally, recent developments of aqueous sodium-ion batteries highlight the use of low-cost and highly stable AC and Prussian Blue anodes; however, both approaches exhibit very low capacities (~50 mAh g^{-1}) (refs 23,24). With the lack of anode materials meeting all requirements, the application of aqueous rechargeable batteries for large-scale energy storage has been stagnant. The major challenges for aqueous anodes lie in the search for materials that are chemically robust towards aqueous electrolytes, easily accessible and inexpensive, have high specific capacity, store charge via a structurally reversible/stable mechanism, and fit in the electrochemical stability window of the electrolyte solvent, thus water.

Quinones, of which the most common motif comprises the 1,2-benzoquinone or 1,4-benzoquinone units (Fig. 1), have been considered for nonaqueous metal-ion batteries and aqueous flow batteries[25–30]. These compounds store charge via an 'ion-coordination' mechanism where the cations coordinate to the negatively charged oxygen atoms upon electrochemical reduction of the carbonyl groups, and uncoordinate reversibly during the reverse oxidation (Fig. 1; not to be confused with quinone derivatives where the carbonyls are converted to redox-inactive groups[31]). Properly functionalized quinones have shown excellent chemical stability[30] and their reduction potentials can be readily tuned from 1.7 to 3.2 V versus Li upon molecular engineering[27]. Despite these advantages, there are only very few pioneering reports on their use in aqueous batteries. Alt *et al.* investigated tetrachloro-1,4-benzoquinone (TCBQ) in 2 M sulfuric acid and demonstrated

[1]Department of Electrical & Computer Engineering and Materials Science and Engineering Program, University of Houston, Houston, Texas 77204, USA. [2]Department of NanoEngineering, University of California, San Diego, California 92093, USA. [3]Department of Chemistry and the Materials Research Center, Northwestern University, Evanston, Illinois 60208, USA. [4]Texas Center for Superconductivity, University of Houston, Houston, Texas 77204, USA. *e-mail: a-facchetti@northwestern.edu; yyao4@uh.edu

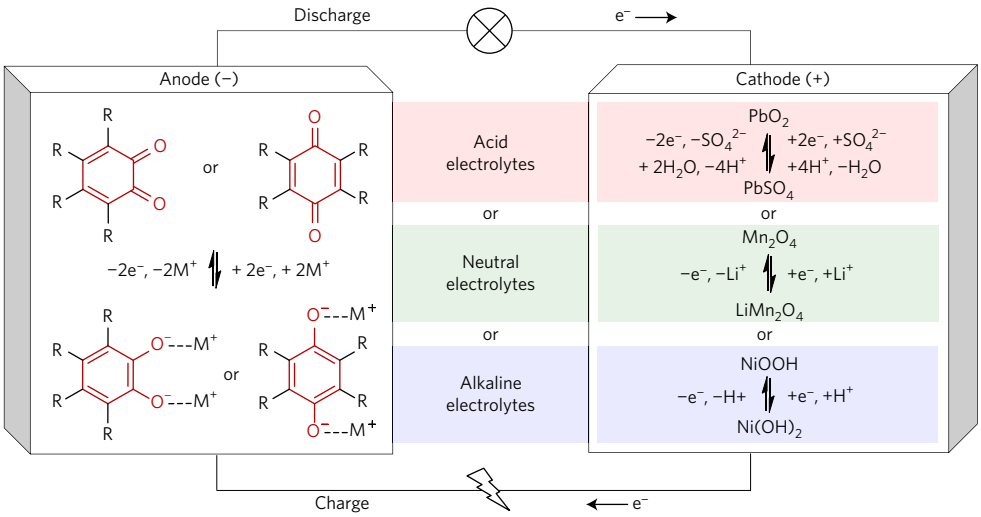

Figure 1 | Schematics of aqueous rechargeable batteries based on quinone anodes operating at different pH values with the indicated corresponding redox chemistries. On the anode side (left panel) is shown the redox/ion-coordination reaction of 1,2-benzoquinone (left) and 1,4-benzoquinone (right) structures. Quinone anodes can be used in acid, neutral, and alkaline electrolytes (middle panel). Depending on the choice of the electrolyte, a wide range of cathode materials including the industrially mature PbO_2 (acid), $LiMn_2O_4$ (neutral), and $Ni(OH)_2$ (alkaline) can be used to complete a battery. The corresponding cathode reactions are shown in the right panel.

stable charge–discharge cycling of 50 cycles[32]. The redox potential of TCBQ is so high (0.91 V versus SHE) that it was used as a cathode material. Nishide's group reported 9,10-anthraquinones as anode materials for alkaline polymer–oxygen batteries[33]; unfortunately, the cell lost 9% of the initial capacity after 300 cycles/25 h.

These works hinted at the promise of quinone redox chemistry and structural stability; however, significant material innovation is needed for optimal performance and broad applicability. Therefore, before the selection/synthetic effort of optimal quinones for our scope, we have identified several guidelines for quinone design. First, the reduction potential should approach, but not be lower than, the potential for the hydrogen evolution reaction [HER, $(-0.059 \times \text{pH})$ V versus SHE] so as to maximize cell voltage without causing water electrolysis. Second, the anode specific capacity should be at least 200 mAh g^{-1} to enhance specific energy. Third, on top of the chemical stability, the solubility of both oxidized /reduced quinone species should be sufficiently low in the selected aqueous electrolytes to prevent material loss by dissolution during cycling[29].

Here we report on the use of quinones as high-performance anode materials for aqueous rechargeable batteries featuring overall characteristics unmet by those deriving from the combination of several other classes. To demonstrate universal generality to the electrolyte medium, quinone anodes were coupled with various industrially mature cathode materials, such as lead oxide (PbO_2, acidic conditions), spinel lithium manganese oxide ($LiMn_2O_4$, near-neutral conditions), and $Ni(OH)_2$ (alkaline conditions) (Fig. 1). Our results demonstrate that cells based on rationally selected/designed quinone anodes exhibit long cycle life (up to 3,000 cycles/3,500 h), high anode specific capacity (up to 200–395 mAh g^{-1}), fast kinetics (67–84% charge/discharge capacity at 10C), and state-of-the-art specific energy/energy densities (up to 76–92 Wh kg^{-1}/161–208 Wh l^{-1}) for several pH conditions (−1 to 15), charge carrier species (H^+, Li^+, Na^+, K^+, Mg^{2+}), temperature (−35 to 25 °C), and atmosphere (with/without O_2).

Quinone selection for different battery technologies

We first report on the selection of suitable quinone structures using an acidic medium and then demonstrate that three quinones are excellent candidates for broad applicability. Details of quinone synthesis are reported in the Supplementary Information (see Synthesis of quinones and Supplementary Figs 1–13 for quinone structural characterization). Briefly, the synthesized quinones (~5 μm in size, Supplementary Fig. 14) were mixed with conductive carbons and pressed into disk electrodes with an active mass ranging from 2.2 to 37 mg cm^{-2}. Electrode/cell fabrication and measurements are described in the Methods section. Coin cells are typically used for both three-electrode half-cell and two-electrode full-cell measurements. Table 1 collects the major performance parameters for the optimal quinones fabricated here as well as those of reference materials operating in acidic (Entries 1–3), slightly acidic (Entry 4), neutral (Entries 5–8), slightly alkaline (Entry 9), and alkaline (Entry 10–12) electrolyte solutions.

Quinone-based acidic batteries

In preliminary experiments the electrochemical reaction of several simple quinones in 4.4 M sulfuric acid (a close approximation of the 'battery acid' used in commercial Pb-acid batteries) was studied. The molecular structures and the potential–capacity data for the more promising quinones are shown in Fig. 2a. Most quinones show a reduction potential within 0.15–0.53 V versus SHE, and theoretical specific capacities of 250–400 mAh g^{-1}. Because the cell voltage is determined by the potential difference between the anode and the cathode, these quinone anodes will enable full-cell voltages of 1.25–1.63 V when coupled with a PbO_2 cathode (1.78 V versus SHE). Such voltages are comparable to the 1.30 V for the AC–PbO_2 hybrid and 25–45% lower than the 2.1 V for Pb–PbO_2. From the plots of Fig. 2b and Supplementary Fig. 15 the plateau-shaped voltage profiles for these quinones clearly provide a stable voltage output, which is far more desirable than the sloping profile for the non-faradaic AC. Among these candidates, pyrene-4,5,9,10-tetraone[34] (PTO, red structure in Fig. 2a) stands out due to the combination of very high theoretical specific capacity (409 mAh g^{-1}) and reasonably low reduction potential (0.5 V versus SHE) (Entry 1 in Table 1). Importantly, the large planar structure of PTO will also render the molecule less soluble than the other quinones, which is an essential feature for stable operation.

The galvanostatic charge–discharge profile of our PTO–PbO_2 acidic cell at 40 mA g^{-1} is shown in Fig. 2b, which exhibits a specific capacity of 395 mAh g^{-1} (>300% and 700% higher than those of Pb and AC, respectively, Fig. 2b and Entries 2 and 3). The very high capacity of PTO effectively compensates the ~0.85 V higher

Table 1 | Electrochemical characteristics, battery configuration and performance parameters of quinones versus other materials.

Entry	pH	Anode	Charge carrier*	Reduction potential*,† (V versus SHE)	Specific capacity* (mAh g^{-1})	Cathode	Specific energy‡ (Wh kg^{-1})	Energy density‡ (Wh l^{-1})	Cycling stability (capacity%@cycle number (cycled time))	Ref.
1	−1	PTO	H^+	0.51	395	PbO_2	76	161	96%@1,500 (1,200 h)	This work
2	−1	Pb	SO_4^{2-}	−0.34	129	PbO_2	78	171	80%@240 (4,500 h)§	7
3	−1	AC	H^+	0.48	50	PbO_2	38	37	83%@3,000 (5,500 h)	13
4	3∼4	PPTO	Mg^{2+}	0.04	144	CuHCF	25	45	66%@1,000 (1,600 h)	This work
5	7	PPTO	Li^+	−0.06	229	$LiMn_2O_4$	92	208	80%@3,000 (3,500 h)	This work
6	7	PPTO	Na^+	−0.07	201	$Na_3V_2(PO_4)_3$	30	80	79%@80 (150 h)	This work
7	7	$LiTi_2(PO_4)_3$	Li^+	−0.52	103	$LiMn_2O_4$	90	243	89%@1,200 (1,600 h)	20
8	7	Polyimide	Li^+	−0.19	160	$LiMn_2O_4$	89	186	70%@50,000 (950 h)	22
9	13	PPTO	Li^+	−0.06	195	$LiCoO_2$	66	180	83%@700 (1,200 h)	This work
10	15	PAQS	K^+	−0.60	200	$Ni(OH)_2$	79	138	88%@1,350 (2,300 h)	This work
11	15	MmH	H^+	−0.81	300	$Ni(OH)_2$	180	597	80%@1,300 (n/a)	45
12	15	Zn	OH^-	−1.19	500	$Ni(OH)_2$	290	714	80%@300 (800 h)	7

*For the anode material. †Determined from three-electrode galvanostatic charge–discharge measurements. ‡For a battery consisting of anode/cathode materials and (if involved in the reaction) electrolyte. §The unusually long time for the small cycle number is due to the slow discharge (C/5) and charge (C/16) required for sustaining cycle life.

redox potential than that of Pb, resulting in uncompromised specific energy. According to the reactions for PTO–PbO_2 (equation (1)) and Pb–PbO_2 (equation (2)) batteries:

$$PbO_2 + 0.5PTO\text{-}H_4 + H_2SO_4 \rightleftharpoons PbSO_4 + 0.5PTO + 2H_2O \quad (1)$$

$$PbO_2 + Pb + 2H_2SO_4 \rightleftharpoons 2PbSO_4 + 2H_2O \quad (2)$$

a PTO–PbO_2 battery requires 50% less sulfuric acid and Pb to store the same amount of charge. The specific energy/energy density of a PTO–PbO_2 battery is 76 Wh kg^{-1}/161 Wh l^{-1} based on active electrode materials and electrolyte (including both solute H_2SO_4 and solvent H_2O). These values are virtually identical to the 78 Wh kg^{-1}/171 Wh l^{-1} for Pb–PbO_2 and much higher than the 38 Wh kg^{-1}/37 Wh l^{-1} for AC–PbO_2. Note that the significantly lower compacted density of PTO than that of Pb (1.65 versus 4.35 g cm^{-3}) does not compromise energy density significantly because PTO, due to its very high specific capacity, constitutes only a considerably small weight fraction (15 wt%) in the battery (compare with 28 wt% for Pb in Pb–PbO_2; the weight fraction breakdown of all battery configurations involved in this work is summarized in Supplementary Table 1). The reduced H_2SO_4 consumption also contributes to the substantial energy density.

A PTO–PbO_2 cell cycles at 100% depth of discharge at 2C charge–discharge rate (1C = 400 mA g^{-1}) for more than 1,500 cycles (>1,200 h) without obvious decrease in capacity and voltage (Fig. 2c and Supplementary Fig. 16). The average coulombic efficiency for the 1,000th–1,500th cycles is 99.8%. The cell is also stable during a longer-term cycling at a low current density of C/5, with 88% capacity retention after 200 cycles (>1,700 h, Supplementary Fig. 17). The stable cycling performance is attributed to three properties of PTO. First, the solubility of PTO in the electrolyte is low (4.7×10^{-6} M; compare with 1.5×10^{-4} M for $PbSO_4$); quinones with higher solubility in acid, for example, 2,5-dihydroxy-1,4-benzoquinone (DHBQ), suffer from fast capacity decay (Supplementary Fig. 18). Second, PTO shows an appreciably high proton diffusivity of 2.32×10^{-9} cm^2 s^{-1} (Supplementary Fig. 19), and therefore does not form ionically insulating layers like $PbSO_4$ does. Third, the electrochemical activity for the charge-transfer reaction of PTO is much higher than that for Pb, as characterized by the much higher exchange current density for a PTO electrode (516.6 mA g^{-1}) than that for Pb (1.41 mA g^{-1}) (ref. 35) (Supplementary Fig. 20). The PTO cell retains 84% of the maximum capacity at a very high charge/discharge rate of 20C (Fig. 2d), sufficient for the demanding scenarios for vehicle batteries such as engine starting (up to 18C pulse discharge) and regenerative breaking (up to 3C pulse charge)[8,36]. Therefore, we have demonstrated that the PTO anode overcomes the passivation and kinetic problems for Pb without sacrificing specific energy/energy density like AC does.

Quinone-based neutral batteries

The results above prompted us to explore quinone anodes for batteries with neutral electrolytes, in particular ALIBs. We found that PTO is soluble in neutral electrolytes and undergoes fast capacity decay (Supplementary Fig. 21), therefore we have designed a polymerized version of PTO, namely PPTO (Fig. 3a), to achieve sufficient insolubility (Entry 5). The electrochemical performance of PPTO is compared with lithium titanium phosphate ($LiTi_2(PO_4)_3$), which is the state-of-the-art anode material for ALIBs (Entry 7). PPTO shows more than double the specific capacity of $LiTi_2(PO_4)_3$ (229 versus 103 mA g^{-1}) albeit 0.46 V higher reduction potential (Fig. 3a). A PPTO–$LiMn_2O_4$ cell shows an average voltage of 1.13 V with a specific energy/energy density of 92 Wh kg^{-1}/208 Wh l^{-1}, which are comparable to those for $LiTi_2(PO_4)_3$-$LiMn_2O_4$ (90 Wh kg^{-1}/243 Wh l^{-1}). Remarkably, PPTO retains 80% of the initial capacity and shows no obvious change in voltage profile after 3,000 deep cycles at 1C (280 mA g^{-1}, Fig. 3c and Supplementary Fig. 22), making it amongst the most stable anode materials for ALIBs discovered to date. Like PTO, PPTO delivers fast electrode kinetics, with 60% of the maximum capacity delivered at 20C charge/discharge (Supplementary Fig. 23a). It is noteworthy that the difference between charge and discharge potentials does not increase with increasing current density, translating into consistently high energy efficiency even during fast charging (Supplementary Fig. 23b).

An important advantage of PPTO over $LiTi_2(PO_4)_3$ and other anode materials reported for ALIBs is its ability to support the 'oxygen cycle', a common phenomenon for all commercial aqueous rechargeable batteries. The oxygen cycle is a built-in safety mechanism where oxygen evolves from water oxidation by the cathode at high charge states, diffuses across the electrolyte, and is reduced by the charged anode (Fig. 3c). Note, the pH of the electrolyte medium decreases/increases near the cathode/anode due to H^+/OH^- formation, respectively. This mechanism spontaneously protects this type of cells from overcharge and helps to synchronize the charge state of all cells in a battery pack. Previously reported ALIBs do not have a proper anode to support the oxygen cycle. $LiTi_2(PO_4)_3$ quickly decays in the presence of oxygen in the electrolyte[9]. Although polyimides are compatible with oxygen

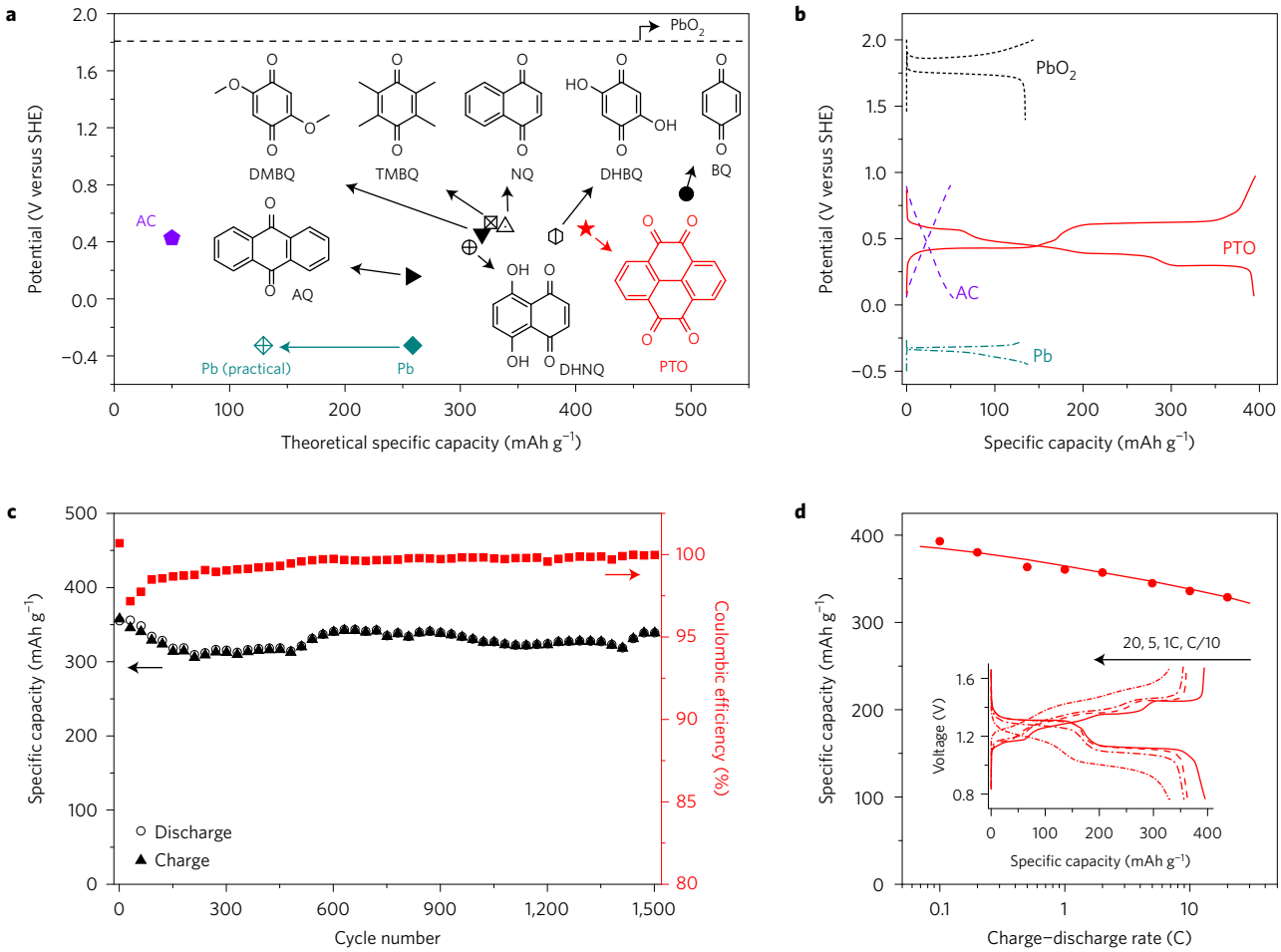

Figure 2 | Quinone-based acidic batteries. a, Chemical structure of selected quinones investigated in this study and their reduction potential and theoretical capacity based on one-carbonyl one-electron reduction. The practical specific capacities of AC and Pb are shown for comparison. Dashed line indicates the reduction potential of PbO_2. **b**, Galvanostatic charge–discharge profiles for PTO (40 mA g^{-1}), AC (50 mA g^{-1}), Pb (10 mA g^{-1}), and PbO_2 (20 mA g^{-1}). **c**, Capacity retention of a PTO–PbO_2 cell during galvanostatic cycling at 2C. **d**, Capacity of a PTO–PbO_2 cell charged/discharged at C/10–20C. Inset shows the voltage profiles at selected C rates. All data were collected in 4.4 M H_2SO_4.

(Entry 8) (ref. 37) they are prone to rapid hydrolysis in the locally alkaline environment resulting from oxygen reduction: naphthalene diimides have half-lives of seconds in moderately alkaline solutions (for example, pH 12) (ref. 38). In contrast, quinones have been reported to show excellent stability in both oxygen[32] and alkaline solutions (for example, 5 M KOH) (ref. 30). PPTO in particular proves to be sufficiently stable in a fairly alkaline electrolyte (pH 13), where it is cycled for more than 1,200 h with a 83% capacity retention (*vide infra*). Such cycling stability originates from the combination of quinone core chemical inertness, PPTO poor solubility, and amide linkage resistance towards hydrolysis in these conditions. Amides of aliphatic acids, which are analogous to PPTO, have half-lives of 240–270 years at neutral pH and about 2–3 years at a pH of 12 (ref. 39). Note that these half-lives are for amides dissolved in solutions (homogeneous reactions), which is a physical state completely different than that of our insoluble PPTO (solid state). Heterogeneous reactions (and hydrolysis in this case) can be orders of magnitude less efficient, if negligible at all. Furthermore, it is reasonable that an anode spends less than 10% of its lifetime under basic conditions, considering that the oxygen cycle takes place only during the high-voltage charging process, thus one can expect a further lifetime extension. If desired, even higher stability may be possible by substituting the intrinsically base-sensitive amide linkage with more stable bridge units/groups via alternative polymerization methods. Reduced (charged) PPTO is reversibly oxidized by oxygen to regenerate PPTO at its discharged state with both the voltage profile and capacity preserved (Fig. 3d). In fact, this oxygen compatibility is a general property of all quinones featured in this work regardless of the pH of the electrolytes (−1 to 15; Supplementary Fig. 24). The oxygen consumption capability of quinones makes it possible to use high-voltage cathode materials[40] that approach the potential for the oxygen evolution reaction (OER), enabling high voltages and specific capacities (Supplementary Fig. 25). An ALIB combining the high-capacity PPTO anode and a high-voltage cathode will yield up to 65% higher specific energy than those of the state-of-the-art ALIBs.

Other aqueous metal-ion batteries enabled by PPTO

In addition to the neutral ALIB described above, we were able to prototype several other interesting aqueous metal-ion batteries based on a PPTO anode and near-neutral electrolytes. This is possible due to the high tolerance of PPTO for electrolytes with different pH and cationic species. Thus, an alkaline ALIB featuring an alkaline Li_2SO_4 electrolyte (pH = 13), PPTO anode, and $LiCoO_2$ cathode (Entry 9) exhibits a high anode specific capacity of 200 mAh g^{-1}, an energy density of 180 Wh l^{-1}, and retains 83% of the initial capacity for more than 700 cycles/1,200 h (Supplementary Fig. 26). Being able to use relatively alkaline electrolytes significantly expands the choice of cathode materials which would otherwise suffer from proton-induced dysfunction in neutral electrolytes[41]. Furthermore,

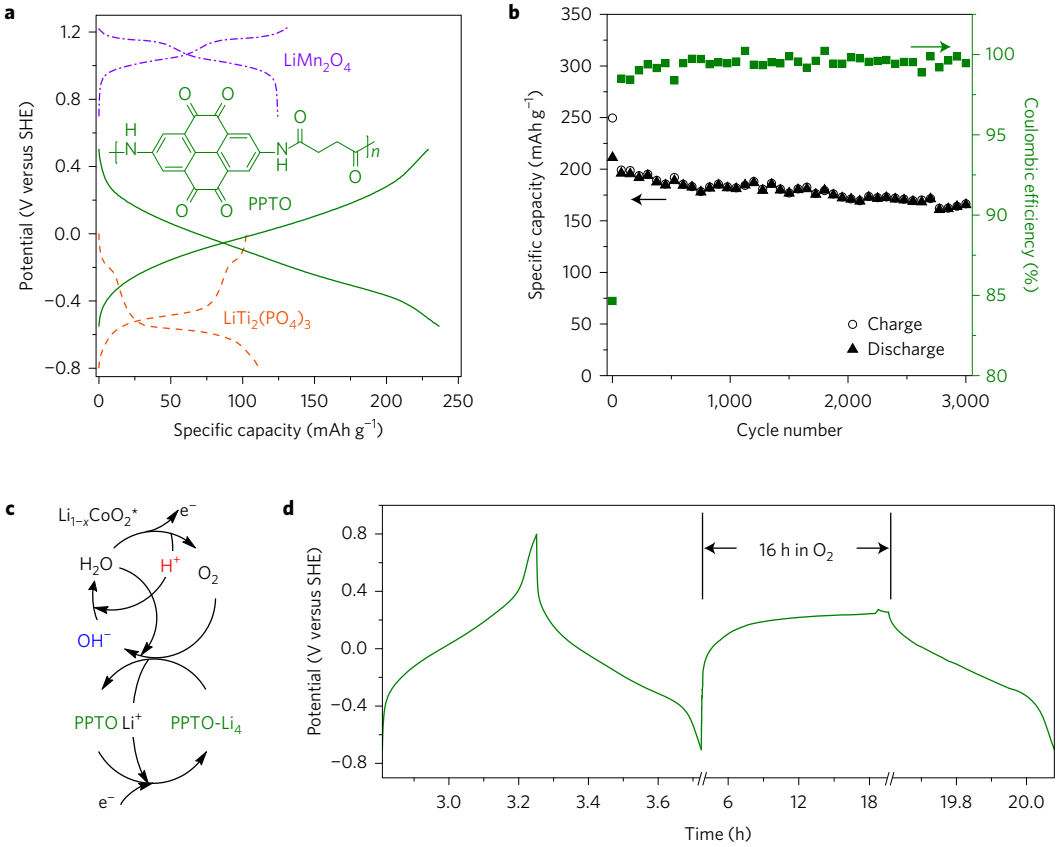

Figure 3 | Quinone-based metal-ion neutral batteries. a, Chemical structure of PPTO. Galvanostatic charge–discharge profiles for PPTO (280 mA g^{-1}), $LiTi_2(PO_4)_3$ (120 mA g^{-1}), and $LiMn_2O_4$ (140 mA g^{-1}) in 2.5 M Li_2SO_4 (pH = 7). **b**, Capacity retention of a $LiMn_2O_4$–PPTO cell during galvanostatic cycling at 1C in 2.5 M Li_2SO_4 (pH 7). **c**, Schematic explaining the oxygen cycle in ALIBs: H_2O is oxidized at the catalytic sites (*) on the cathode (for example, $LiCoO_2$) to generate O_2 and H^+; the latter is then reduced by the charged anode (for example, PPTO-Li_4) to afford OH^-. **d**, Oxygen consumption by charged PPTO: a PPTO electrode is first electrochemically discharged (oxidized) and charged (reduced) under Ar for one cycle, then left to rest under O_2, and finally put under Ar and charged again.

we replaced lithium in ALIBs with the low-cost and Earth-abundant sodium to construct aqueous sodium-ion batteries (ASIBs)[23,42]. This technology may find application in areas where cost and stability, and not energy density, may be of primary importance. A prototype quinone-based ASIB with the PPTO–sodium vanadium phosphate ($Na_3V_2(PO_4)_3$) configuration shows high anode specific capacity (201 mAh g^{-1}) and 79% retention after 80 cycles in a neutral sodium nitrate electrolyte (Entry 6, Supplementary Fig. 27), although the energy density (80 Wh l^{-1}) is modest as limited by the low specific capacity and potential of $Na_3V_2(PO_4)_3$ (52 mAh g^{-1} at 0.65 V versus SHE). Finally, we have explored for the first time the feasibility of an aqueous magnesium-ion battery (AMIB). The success of an AMIB relies on the acid compatibility of PPTO (Entry 4 and Supplementary Fig. 28) considering that all aqueous magnesium electrolytes are noticeably acidic due to partial Mg^{2+} hydrolysis. We have assembled an AMIB using PPTO as the anode and a Prussian blue analogue/magnesiated copper hexacyanoferrate (Mg_xCuHCF) (ref. 43) as the cathode which shows stable cycling performance (66% retention after 1,000 cycles) and uncommonly fast kinetics for a rechargeable magnesium battery (85% of maximum capacity at 2C; 1C = 140 mA g^{-1}; Supplementary Fig. 29).

Quinone-based alkaline batteries

We further expanded quinone anodes in even more alkaline electrolytes (pH > 14) in conjunction with the highly industrially mature $Ni(OH)_2$/nickel oxyhydroxide (NiOOH) cathode (Entry 10). Since alkaline electrolytes have low-lying HER potentials, our quinone of choice for an alkaline battery is an anthraquinone-based polymer, poly(anthraquinonyl sulfide)[44] (PAQS), which has a 0.54 V more negative reduction potential than that of PPTO. The reactions for PAQS–$Ni(OH)_2$ (equation (3)) and MmH–$Ni(OH)_2$ (equation (4)) are

$$Ni(OH)_2 + (0.5/n)PAQS + KOH \rightleftharpoons NiOOH + (0.5/n)PAQS\text{-}K_2 + 2H_2O \quad (3)$$

$$Ni(OH)_2 + Mm \rightleftharpoons NiOOH + MmH \quad (4)$$

where n is the degree of polymerization of PAQS. At room temperature, PAQS shows a specific capacity of 200 mAh g^{-1} in 10 M potassium hydroxide (KOH) (Fig. 4a). Because of the consumption of the KOH electrolyte, the specific energy/energy density of PAQS–$Ni(OH)_2$ (79 Wh kg^{-1}/138 Wh l^{-1}) are not as high as those of MmH–$Ni(OH)_2$ (~180 Wh kg^{-1}/597 Wh l^{-1}; Entry 11) but comparable to those of PTO–PbO_2. By comparing the voltage profiles of PAQS and MmH electrodes it is clear that there is much room for further lowering the reduction potential of the quinone anode before hydrogen would evolve. For example, a quinone with the capacity of PTO but a reduction potential 0.2 V lower than that of PAQS would yield much higher specific energy/energy density of 115 Wh kg^{-1}/203 Wh l^{-1}. A PAQS–$Ni(OH)_2$ cell cycled at 100% depth of discharge for 1,350 cycles at 1C (200 mA g^{-1}) with an 88% capacity retention (Fig. 4b). The absence of noticeable change in the charge–discharge profile (Supplementary Fig. 30) after prolonged cycling reflects the excellent stability of the electrode in these extreme conditions. Such stability

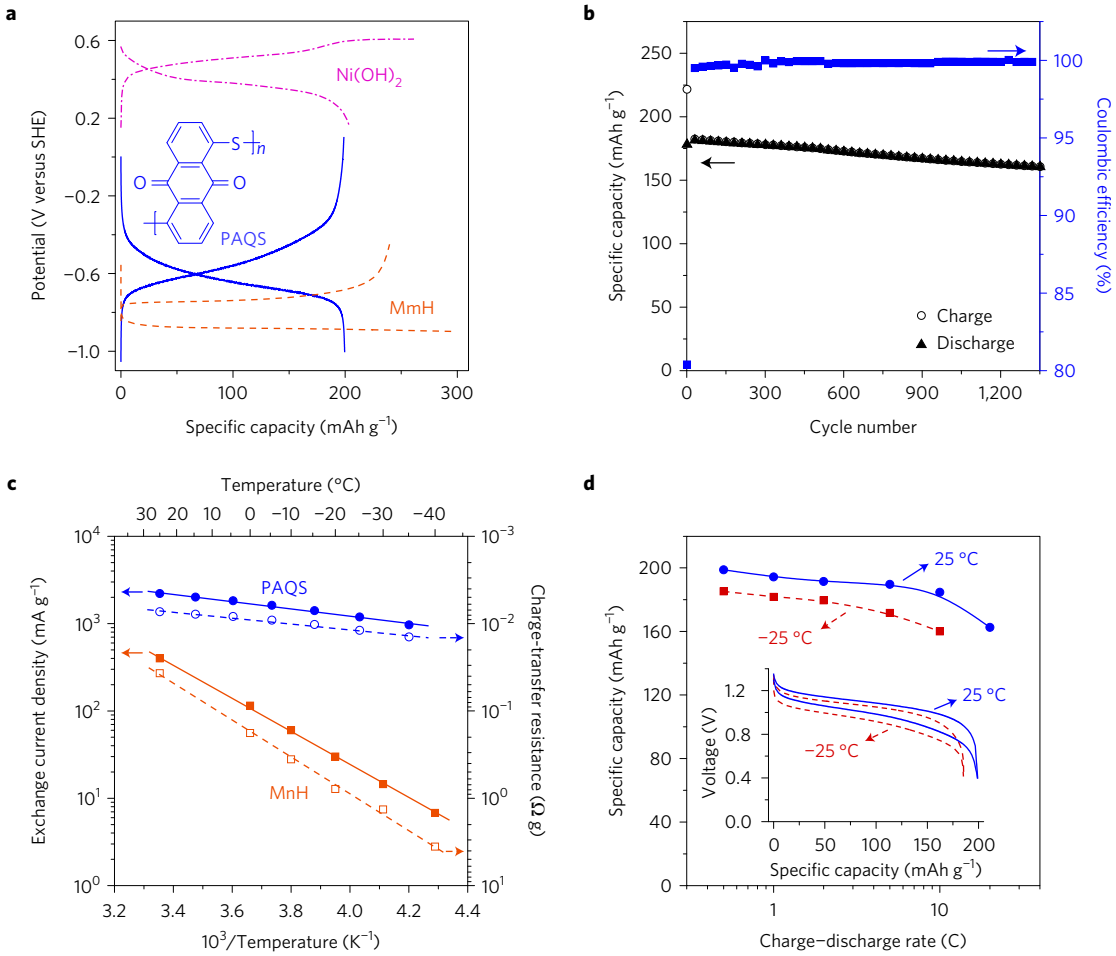

Figure 4 | Quinone-based alkaline batteries. a, Galvanostatic charge–discharge profiles of PAQS (100 mA g^{-1}), MmH (150 mA g^{-1}), and $Ni(OH)_2$ (40 mA g^{-1}). **b**, Capacity retention of a PAQS–$Ni(OH)_2$ cell during galvanostatic cycling at 1C. **c**, Exchange current density and charge-transfer resistance of PAQS and MmH electrodes as a function of temperature (data for MmH retrieved from ref. 48). **d**, Capacity of a PAQS–$Ni(OH)_2$ cell charged/discharged at C/2–20C at 25 °C and C/2–10C at −25 °C. Inset shows the voltage profiles at C/2. All data here were collected in 10 M KOH.

outperforms those of the most optimized metal hydrides (80% retention after 1,300 cycles[45]). Like PPTO, PAQS also functions with various metal cations. Sodium hydroxide and lithium hydroxide are both plausible electrolytes for a PAQS–$Ni(OH)_2$ battery in addition to KOH (Supplementary Fig. 31). Such a tolerance allows the use of mixed hydroxide electrolytes to customize battery performance, a common practice for the nickel–metal hydride battery technology[46].

PAQS also addresses one of the major disadvantages of nickel–MmH batteries—that is, drastic reduction in electrochemical performance at low temperatures. Most commercial MmH–$Ni(OH)_2$ batteries deliver only ∼50% of the nominal energy and can rarely discharge beyond C/2 at −25 °C (ref. 47). This performance reduction originates from the large charge-transfer resistance for the redox reaction of MmH, which increases by 100× as temperature decreases from 25 to −40 °C (ref. 48). In comparison, the charge-transfer resistance for PAQS only doubles from 25 to −35 °C (characterized by electrochemical impedance spectroscopy; Fig. 4c and Supplementary Fig. 32a). The activation energy for the redox reaction of PAQS, calculated from the Arrhenius equation of the charge-transfer resistance versus temperature dependence, is as low as 8 kJ mol^{-1} (compare with 39 kJ mol^{-1} for MmH), implying little performance dependence on temperature. The exchange current density of the two electrodes reiterates the different dependence of the electrochemical activity on temperature for the two materials (Fig. 4c and Supplementary Fig. 32b). Consequently, PAQS experiences a mere 7% reduction in capacity as the temperature decreases from 25 to −25 °C, and the voltage gap between charge and discharge at C/2 (1C = 225 mA g^{-1}) increases only slightly from 101 to 127 mV (Fig. 4d). Importantly, the rate capability of PAQS is consistently high regardless of temperature, with 93 and 86% capacity remaining at 10C charge/discharge at 25 and −25 °C, respectively (Fig. 4d and Supplementary Fig. 33).

Challenges and opportunities of quinone anodes

Figure 5a summarizes the reduction potential versus pH of PTO, PPTO, and PAQS electrodes in a Pourbaix diagram. The media at which our quinones operate span a very wide pH range, from strongly acidic through neutral to strongly alkaline. From the plot it is clear that at every pH value these quinones approach the HER potential and still have room for further improvement. For $-1 < pH < 1$, the reduction potentials of all three quinones are pH-dependent and decrease by 59 mV per pH increment, indicating a proton storage mechanism where one proton is stored for every injected electron and vice versa. As the pH increases above 3, the concentration of proton decreases to such an extent that metal-ion storage becomes dominant and the reduction potential becomes pH-independent. Indeed, compositional analysis via inductively coupled plasma method for a PPTO electrode charged (electrochemically reduced) in a Li_2SO_4 (pH 7) electrolyte solution was performed and confirmed that virtually all (∼97%) of the injected charge was balanced by lithium ions instead of protons (see details in Methods).

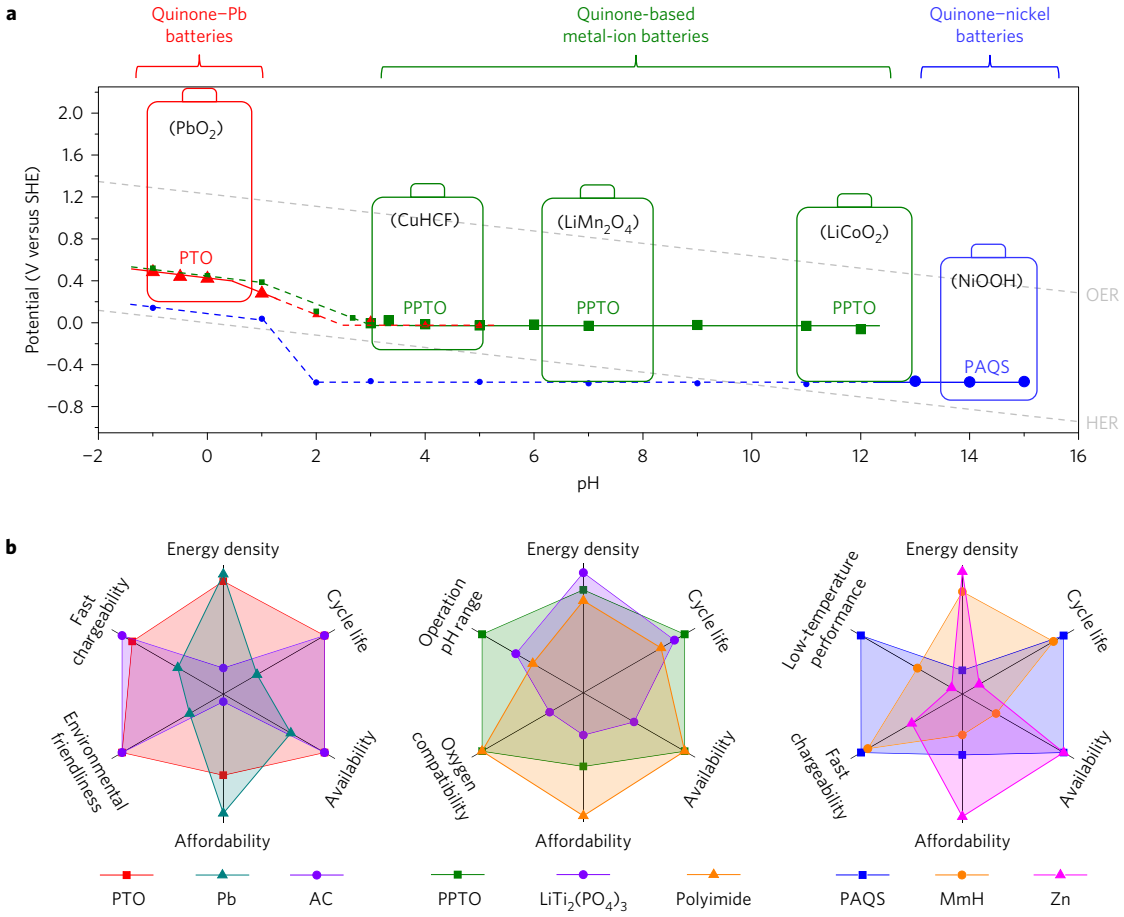

Figure 5 | Comparison of anode materials for aqueous rechargeable batteries. a, Correlation between the reduction potentials of quinone electrodes measured with cyclic voltammetry and the pH value of aqueous electrolytes. The battery drawings depict plausible battery configurations based on quinone anodes and suitable cathodes. They are positioned at the pH range where the described batteries operate. The top and bottom of the battery drawings denote the end-of-charge potential for the cathode and anode, respectively. Larger symbols highlight the data points directly related to the quinone–pH combinations studied in the batteries. Grey dashed lines show the thermodynamic potential for O_2 (OER) and H_2 (HER) evolution with pH. **b**, Itemized comparison of quinones with existing anode materials for acidic batteries (AC and Pb), ALIBs ($LiTi_2(PO_4)_3$ and imide), and alkaline batteries (MmH and Zn).

Finally, Fig. 5b and Supplementary Table 2 compare some of the most important electrode parameters for quinones and competing commercial and emerging anode materials, including Pb, AC (both for acidic batteries), $LiTi_2(PO_4)_3$, polyimide (both for ALIBs), MmH, and Zn (Entry 12) (both for alkaline batteries). Quinone anodes deliver specific capacity and energy density values that can match or exceed those of several existing anode materials (Supplementary Fig. 34a). However, structural modification of these quinoid cores/structures with, for instance, simple electron-donating organic functionalities can overcome one of the major limitations of the three examples reported here, which is the relatively high reduction potential. Thus, optimized quinones retaining PTO specific capacity but with lower reduction potentials combined with reasonably improved cathodes may further increase the specific energy/energy density of quinone-based batteries to 115–228 Wh kg^{-1}/203–522 Wh l^{-1}, most of which values are unachievable with other existing anodes (Supplementary Fig. 34b). Furthermore, polymerization protocols affording macromolecules with even higher molecular weights, thus lower solubility, as well as different quinone unit connectivities could further enhance cell stability. However, our quinones already clearly demonstrate excellent cycle life and without availability/cost/environmental issues that some heavy metals and phosphates experience[49,50]. Their fast electrode kinetics and efficient charge transport ensure high power and fast chargeability even at low temperatures; hence, overcoming some of the major obstacles for existing acid and alkaline batteries. Their support for the oxygen cycle further adds the critically important reliability to neutral aqueous rechargeable batteries, paving the way towards their practical application.

In conclusion, this work demonstrates that regardless of the pH of the medium, charge carrier species, temperature, and atmosphere, quinones can be designed to operate as stable anode materials. Quinone anodes can be coupled with any cathode/electrolyte combinations for aqueous rechargeable batteries. They enable batteries with long cycle life, high capacity, fast kinetics, as well as several examples of excellent energy density values, rendering them viable contenders for large-scale energy storage. Furthermore, the possibility of structural modifications of quinone cores with electron-withdrawing and/or electron-donating substituents and variation of the polymerization protocols provides an opportunity to improve cell performance and stability further.

Methods

Methods, including statements of data availability and any associated accession codes and references, are available in the online version of this paper.

Received 11 November 2016; accepted 18 April 2017; published online 19 June 2017

References

1. Dunn, B., Kamath, H. & Tarascon, J.-M. Electrical energy storage for the grid: a battery of choices. *Science* **334,** 928–935 (2011).
2. Goodenough, J. B. & Manthiram, A. A perspective on electrical energy storage. *MRS Commun.* **4,** 135–142 (2014).
3. Liu, P., Ross, R. & Newman, A. Long-range, low-cost electric vehicles enabled by robust energy storage. *MRS Energy Sustain.* **2,** E12 (2015).
4. Kim, H. *et al*. Aqueous rechargeable Li and Na ion batteries. *Chem. Rev.* **114,** 11788–11827 (2014).
5. Pan, H. *et al*. Reversible aqueous zinc/manganese oxide energy storage from conversion reactions. *Nat. Energy* **1,** 16039 (2016).
6. Kundu, D. *et al*. A high-capacity and long-life aqueous rechargeable zinc battery using a metal oxide intercalation cathode. *Nat. Energy* **1,** 16119 (2016).
7. Reddy, T. B. *Linden's Handbook of Batteries* 4th edn (McGraw-Hill, 2011).
8. Lam, L. T., Haigh, N. P., Phyland, C. G. & Urban, A. J. Failure mode of valve-regulated lead-acid batteries under high-rate partial-state-of-charge operation. *J. Power Sources* **133,** 126–134 (2004).
9. Luo, J. Y., Cui, W. J., He, P. & Xia, Y. Y. Raising the cycling stability of aqueous lithium-ion batteries by eliminating oxygen in the electrolyte. *Nat. Chem.* **2,** 760–765 (2010).
10. Shukla, A. K., Venugopalan, S. & Hariprakash, B. Nickel-based rechargeable batteries. *J. Power Sources* **100,** 125–148 (2001).
11. Lam, L. T. *et al*. VRLA Ultrabattery for high-rate partial-state-of-charge operation. *J. Power Sources* **174,** 16–29 (2007).
12. Buiel, E. R. *et al*. Cell assembly for an energy storage device with activated carbon electrodes. US patent US 7881042 B2 (2011).
13. Yu, N., Gao, L., Zhao, S. & Wang, Z. Electrodeposited PbO_2 thin film as positive electrode in PbO_2/AC hybrid capacitor. *Electrochim. Acta* **54,** 3835–3841 (2009).
14. Lei, D. *et al*. Performance enhancement and side reactions in rechargeable nickel–iron batteries with nanostructured electrodes. *ACS Appl. Mater. Interfaces* **8,** 2088–2096 (2016).
15. Ying, T. K. *et al*. Studies on rechargeable NiMH batteries. *Int. J. Hydrog. Energy* **31,** 525–530 (2006).
16. Li, W., Dahn, J. R. & Wainwright, D. S. Rechargeable lithium batteries with aqueous electrolytes. *Science* **264,** 1115–1118 (1994).
17. Suo, L. *et al*. "Water-in-salt" electrolyte enables high-voltage aqueous lithium-ion chemistries. *Science* **350,** 938–943 (2015).
18. Levi, M. D. *et al*. Ultrafast anode for high voltage aqueous Li-ion batteries. *J. Solid State Electrochem.* **16,** 3443–3448 (2012).
19. Wu, Y. P. *et al*. Aqueous rechargeable lithium batteries as an energy storage system of superfast charging like filling gasoline. *Energy Environ. Sci.* **6,** 2093–2104 (2013).
20. Sun, D. *et al*. Long-lived aqueous rechargeable lithium batteries using mesoporous $LiTi_2(PO_4)_3$@C anode. *Sci. Rep.* **5,** 17452 (2015).
21. Qin, H., Song, Z. P., Zhan, H. & Zhou, Y. H. Aqueous rechargeable alkali-ion batteries with polyimide anode. *J. Power Sources* **249,** 367–372 (2014).
22. Dong, X. *et al*. Environmentally-friendly aqueous Li (or Na)-ion battery with fast electrode kinetics and super-long life. *Sci. Adv.* **2,** e1501038 (2016).
23. Whitacre, J. F. *et al*. An aqueous electrolyte, sodium ion functional, large format energy storage device for stationary applications. *J. Power Sources* **213,** 255–264 (2012).
24. Pasta, M. *et al*. Full open-framework batteries for stationary energy storage. *Nat. Commun.* **5,** 3007 (2014).
25. Milczarek, G. & Inganäs, O. Renewable cathode materials from biopolymer/conjugated polymer interpenetrating networks. *Science* **335,** 1468–1471 (2012).
26. Poizot, P. & Dolhem, F. Clean energy new deal for a sustainable world: from non-CO_2 generating energy sources to greener electrochemical storage devices. *Energy Environ. Sci.* **4,** 2003–2019 (2011).
27. Liang, Y., Tao, Z. & Chen, J. Organic electrode materials for rechargeable lithium batteries. *Adv. Energy Mater.* **2,** 742–769 (2012).
28. Liang, Y. *et al*. Heavily n-dopable π-conjugated redox polymers with ultrafast energy storage capability. *J. Am. Chem. Soc.* **137,** 4956–4959 (2015).
29. Muench, S. *et al*. Polymer-based organic batteries. *Chem. Rev.* **116,** 9438–9484 (2016).
30. Lin, K. *et al*. Alkaline quinone flow battery. *Science* **349,** 1529–1532 (2015).
31. Haupler, B. *et al*. Aqueous zinc-organic polymer battery with a high rate performance and long lifetime. *NPG Asia Mater.* **8,** e283 (2016).
32. Alt, H., Binder, H., Köhling, A. & Sandstede, G. Investigation into the use of quinone compounds-for battery cathodes. *Electrochim. Acta* **17,** 873–887 (1972).
33. Choi, W., Harada, D., Oyaizu, K. & Nishide, H. Aqueous electrochemistry of poly(vinylanthraquinone) for anode-active materials in high-density and rechargeable polymer/air batteries. *J. Am. Chem. Soc.* **133,** 19839–19843 (2011).
34. Liang, Y., Zhang, P. & Chen, J. Function-oriented design of conjugated carbonyl compound electrodes for high energy lithium batteries. *Chem. Sci.* **4,** 1330–1337 (2013).
35. Vijayasekaran, B. & Basha, C. A. Shrinking core discharge model for the negative electrode of a lead-acid battery. *J. Power Sources* **158,** 710–721 (2006).
36. Moseley, P. T. High rate partial-state-of-charge operation of VRLA batteries. *J. Power Sources* **127,** 27–32 (2004).
37. Chen, L. *et al*. Aqueous lithium-ion batteries using O_2 self-elimination polyimides electrodes. *J. Electrochem. Soc.* **162,** A1972–A1977 (2015).
38. Kim, M. B. & Dixon, D. W. Hydrolysis of aliphatic naphthalene diimides: effect of charge placement in the side chains. *J. Phys. Org. Chem.* **21,** 731–737 (2008).
39. Smith, R. M. & Hansen, D. E. The pH-rate profile for the hydrolysis of a peptide bond. *J. Am. Chem. Soc.* **120,** 8910–8913 (1998).
40. Freire, M. *et al*. A new active Li-Mn-O compound for high energy density Li-ion batteries. *Nat. Mater.* **15,** 173–177 (2016).
41. Shu, Q. *et al*. Proton-induced dysfunction mechanism of cathodes in an aqueous lithium ion battery. *J. Phys. Chem. C* **117,** 6929–6932 (2013).
42. Wang, Y. *et al*. Ti-substituted tunnel-type $Na_{0.44}MnO_2$ oxide as a negative electrode for aqueous sodium-ion batteries. *Nat. Commun.* **6,** 6401 (2015).
43. Wang, R. Y., Wessells, C. D., Huggins, R. A. & Cui, Y. Highly reversible open framework nanoscale electrodes for divalent Ion batteries. *Nano Lett.* **13,** 5748–5752 (2013).
44. Song, Z. *et al*. Polymer–graphene nanocomposites as ultrafast-charge and -discharge cathodes for rechargeable lithium batteries. *Nano Lett.* **12,** 2205–2211 (2012).
45. Bäuerlein, P., Antonius, C., Löffler, J. & Kümpers, J. Progress in high-power nickel–metal hydride batteries. *J. Power Sources* **176,** 547–554 (2008).
46. Rubin, E. J. & Baboian, R. A correlation of the solution properties and the electrochemical behavior of the nickel hydroxide electrode in binary aqueous alkali hydroxides. *J. Electrochem. Soc.* **118,** 428–433 (1971).
47. Pierozynski, B. On the low temperature performance of nickel-metal hydride (NiMH) batteries. *Int. J. Electrochem. Sci.* **6,** 860–866 (2011).
48. Senoh, H., Hara, Y., Inoue, H. & Iwakura, C. Charge efficiency of misch metal-based hydrogen storage alloy electrodes at relatively low temperatures. *Electrochim. Acta* **46,** 967–971 (2001).
49. Vesborg, P. C. K. & Jaramillo, T. F. Addressing the terawatt challenge: scalability in the supply of chemical elements for renewable energy. *RSC Adv.* **2,** 7933–7947 (2012).
50. Cordell, D. & White, S. Peak phosphorus: clarifying the key issues of a vigorous debate about long-term phosphorus security. *Sustainability* **3,** 2027–2049 (2011).

Acknowledgements

The information, data, or work presented herein was funded in part by the Advanced Research Projects Agency-Energy (ARPA-E), US Department of Energy, under Award Number DE-AR0000380. The aqueous Mg-ion battery study was supported by the Office of Naval Research Young Investigator Award (N00014-13-1-0543). The aqueous Na-ion battery study was supported by the National Science Foundation (NSF CMMI-1400261). This research used resources of the Advanced Photon Source, a US Department of Energy (DOE) Office of Science User Facility operated for the DOE Office of Science by Argonne National Laboratory under Contract No. DE-AC02-06CH11357. A.F. thanks the Shenzhen Peacock Plan project (KQTD20140630110339343) for support. We thank J. Xu and E. R. Buiel for helpful discussions and Z. Meng for the help on fabricating alkaline batteries.

Author contributions

Y.Y. and Y.L. conceived this work; Y.L., P.L. and Y.Y. designed the experiments; Y.L., Y.J. and S.G. synthesized the materials; Y.L., Y.J., S.G. and K.-Y.L. carried out the electrochemical measurements; A.F. and Y.L. performed the battery material cost analysis; Y.Y. and A.F. directed the project; Y.L., A.F. and Y.Y. co-wrote the paper; all authors analysed the results and commented on the manuscript.

Additional information

Supplementary information is available in the online version of the paper. Reprints and permissions information is available online at www.nature.com/reprints. Publisher's note: Springer Nature remains neutral with regard to jurisdictional claims in published maps and institutional affiliations. Correspondence and requests for materials should be addressed to A.F. or Y.Y.

Competing financial interests

Y.Y. and Y.L. are inventors of patent applications (US/2014/0308581, US/2016/0049659) on the neutral and alkaline batteries described herein. Y.Y., Y.L., S.G. and Y.J. are inventors of a patent application (US/62/165,377) on the acid batteries. A.F. has no competing interests.

Methods

Fabrication of quinone electrodes. Quinones shown in Fig. 2a were mixed with hydrophilic multi-walled carbon nanotubes (COOH-functionalized, 10–30 μm in length, 20–30 nm in diameter; US Research Nanomaterials) in a 1:1 ratio (all ratios are reported by weight unless specified otherwise)[14] with the aid of H_2O, dried under vacuum, and pressed to form disk electrodes with the areal mass loading being 16 mg cm^{-2}. PPTO, Super P carbon (TIMCAL), and polytetrafluoroethylene (MTI) were mixed in a 6:3:1 ratio with the aid of ethanol, pressed into a stainless steel mesh disk (type 316), and dried in vacuum. The areal mass loading of PPTO in the electrode is 2.2 mg cm^{-2}. PAQS, Super P carbon, and polytetrafluoroethylene were mixed in a 7:2:1 ratio with the aid of H_2O, and the resulting mixture was pressed and dried under vacuum to form electrodes. The areal mass loading of PAQS in the electrode is 37 mg cm^{-2}. The Pb electrode was cut from a commercial Pb-acid battery. Activated carbon (AC) cloth (KYNOL) was used as the electrode as received. Carbon-coated $LiTi_2(PO_4)_3$ was synthesized as previously reported[51]. The $LiTi_2(PO_4)_3$ electrode was fabricated via a procedure similar to that for PPTO but with a 7:2:1 ratio. The Mischmetal electrode was fabricated by spreading a slurry of $MmNi_{3.69}Co_{0.72}Mn_{0.40}Al_{0.21}X$ (CXTC), Ni (T255), carboxymethyl cellulose, polyacrylate sodium, and styrene-butadiene rubber (10:0.1:0.009:0.012:0.525) in H_2O onto nickel foam followed by drying and pressing. The electrode was activated by galvanostatically charging–discharging at 75 mA g^{-1} for 10 cycles and then 150 mA g^{-1} for 5 cycles in 8 M KOH.

Half-cell measurements. Three-electrode half-cell measurements were performed to determine the dependence of reduction potentials of quinones on pH and the voltage profiles of individual electrode materials. In particular, the former was measured by cyclic voltammogram and the latter by galvanostatic charge–discharge. Coin cells (CR2032) were used to perform the three-electrode measurements. The electrodes of interest were placed at the positive side as the working electrode. Activated carbon cloth served as the counter electrode at the negative side. For pH −1 to 13, Ag/AgCl (0.197 V versus SHE) served as the reference electrode. For more alkaline electrolytes, Hg/HgO (0.098 V versus SHE) was used instead. The reference electrodes connected to the electrolyte via a hole at the negative case. For pH < 1, H_2SO_4 with the desired concentration in H_2O was used as the electrolyte. For pH from 1 to 13, 1 M KCl with calculated amount of H_2SO_4 and LiOH were the electrolytes for PTO and PAQS. For PPTO studies, the supporting electrolyte KCl was replaced by 2.5 M Li_2SO_4. For pH > 13, KOH with the desired concentration in H_2O was used as the electrolyte. Galvanostatic intermittent titration technique (GITT) was used to determine the proton diffusivity in PTO/PTO-H_x. A cycled PTO electrode was first fully discharged (oxidized). The electrode was then charged at 600 mA g^{-1} for 108 s and then left for rest for 30 min. The charging–resting was repeated until the charge potential reached 0.3 V versus SHE. The ion diffusivity was calculated as reported[28].

Full-cell measurements. The cycling performance, rate capability, and temperature-dependent properties were measured with two-electrode full-cell set-ups. The quinone anode is the capacity-limiting component in each of the full cells. The cathodes were brought to 50% state of charge before coupling with a quinone electrode. $PbO_2/PbSO_4$ and $NiOOH/Ni(OH)_2$ electrodes were taken from commercial batteries. $LiMn_2O_4$ electrodes were fabricated as previously reported[52]. The $LiCoO_2/Li_xCoO_2$ electrode was fabricated from $LiCoO_2$ powder (MTI) via a procedure similar to that for PAQS but with an 8:1:1 ratio. $Na_3V_2(PO_4)_3$ (ref. 53) and CuHCF (ref. 54) were synthesized and the corresponding electrodes fabricated according to reported methods. Glass fibre paper was used as the separator for acid and near-neutral batteries, while polyamide separator was used for alkaline batteries. The separators were wetted with the following electrolytes: 4.4 M H_2SO_4 for acid batteries; 2.5 M Li_2SO_4 (pH 7 and 13), 5 M $NaNO_3$, 4.5 M $Mg(NO_3)_2$ for aqueous lithium-ion, sodium-ion, and magnesium-ion batteries, respectively; 10 M KOH for alkaline batteries. Swagelok-type cells were used for acid batteries, where Pb and titanium were the current collectors for the cathode and anode, respectively. Coin cells were used for all other battery configurations.

Exchange current density of PTO electrodes. The exchange current density of PTO electrodes was measured with micro-polarization. A cycled PTO–PbO_2 cell was brought to 38% state of charge, left for rest for 30 min, and then scanned at 1 mV s^{-1} in the range of ±3 mV versus the equilibrium voltage. The exchange current density (J_0) is derived from the slope according to $J_0 = J\,R\,T/(F\Delta V)$, where J is the measured current, R is the gas constant, T is the temperature, F is the faradaic constant, and ΔV is the voltage perturbation.

Temperature-dependent properties of PAQS electrodes. The temperature-dependent properties of PAQS electrodes were characterized by exchange current density and charge-transfer resistance measured with micro-polarization and electrochemical impedance spectroscopy, respectively. A cycled PAQS–AC cell was brought to 50% state of charge at room temperature. The cell was then brought to the desired temperature and left to rest for 30 min prior to measurements. Electrochemical impedance measurements were performed from 100 kHz to 5 mHz with a perturbation voltage of 3 mV. The charge-transfer resistance was fitted from the semicircle at mid frequency. The activation energy was calculated from either exchange current density or charge-transfer resistance using the Arrhenius equation.

Electrode composition analysis. The intercalating ion species in PPTO charged in 2.5 M Li_2SO_4 was analysed with the inductively coupled plasma (ICP) technique. The fabrication of electrode and cell followed the typical procedure described above, except that 5 wt% of calcium carbonate was added to the electrode mixture as an inert internal reference. The cell was disassembled at the fully charged (lithiated) state. The electrolyte on the surface of the PPTO electrode was briefly absorbed with weighing paper. The mixture was scraped from the stainless steel mesh current collector, dried, and digested for analysis. There are two types of lithium ions in the electrode: the lithium ions coordinated to PPTO and those from residual Li_2SO_4. The latter is subtracted by measuring the concentration of sulfur: Li_2SO_4 is the only species in the cell that contains sulfur, and the atomic ratio of Li:S is 2:1. The ratio of coordinated lithium to the host PPTO cannot be directly determined because none of the elements in PPTO (carbon, hydrogen, oxygen, and nitrogen) is measurable with ICP. The internal reference calcium carbonate is therefore used to indicate the PPTO concentration in the sample solution. The use of an internal reference ensures accurate measurement of lithium content despite incomplete transfer of the electrode material from the current collector.

Energy and power calculations. The specific energy of a cell configuration (E_s) is calculated as the product of the cell voltage (V_{cell}) and cell specific capacity (C_{cell}) following the recent review paper 'Polymer-based organic batteries' from U. S. Schubert's group[29]

$$E_s = C_{cell} \times V_{cell} \tag{5}$$

C_{cell} is typically calculated from the specific capacities of cathode (C_c) and anode (C_a)

$$C_{cell} = (C_c^{-1} + C_a^{-1})^{-1} \tag{6}$$

Note that C_{cell} is calculated based on the weight of active materials—that is, the weight of inert components such as packaging materials, separator, conductive agent, current collectors, and so on is not included. Therefore E_s is the maximum specific energy that can be delivered by a cell configuration. A rough estimation of actual specific energy is to consider that the inert components add ~100% weight to active materials, thus halving the specific energy from the maximum[7]. The weight of electrolytes needs to be included for calculation when the electrolyte is consumed in the battery reaction (that is, acid batteries of all forms and quinone–nickel batteries), thus

$$C_{cell} = (C_c^{-1} + C_a^{-1} + C_e^{-1})^{-1} \tag{7}$$

where C_e is the 'apparent specific capacity' of the electrolyte, which is defined as

$$C_e = z \times F/(M_w \times c^{-1}) \tag{8}$$

where M_w is the molecular weight of the solute that participates in the reaction (for example, H_2SO_4 and KOH), z is the mole number of electrons transferred with the consumption of one mole of electrolyte solute molecule (for example, $z = 1$ for Pb–PbO_2 and $z = 2$ for PTO–PbO_2), F is the Faraday constant, and c is the mass concentration of the electrolyte. V_{cell} is theoretically the difference between the potential of cathode (E_c) and anode (E_a)

$$V_{cell} = E_c - E_a \tag{9}$$

Experimentally, V_{cell} is usually obtained as the average voltage between charge and discharge. Specifically for plotting the Ragone plot (Supplementary Fig. 14a), the cell voltage is defined as the discharge voltage so as to reflect the change of output voltage as the current density changes. Because of the lack of current density-dependent voltage data for some cell configurations reported in literature, up to 10% overestimation of specific energy should be expected in the Ragone plot for non-quinone-based batteries. In the end, the universal equation for E_s is expressed as

$$E_s = (C_c^{-1} + C_a^{-1} + C_e^{-1})^{-1} \times V_{cell} \tag{10}$$

Energy density (E_d) is defined as energy per total volume of cathode/anode materials and, if involved in the reaction, electrolytes:

$$E_d = \text{Energy}/\text{Volume} \tag{11}$$

$$= (\text{Capacity} \times V_{cell})/(V_c + V_a + V_e) \tag{12}$$

$$= [C_{cell} \times (W_c + W_a + W_e) \times V_{cell}]/(W_c/\rho_c + W_a/\rho_a + W_e/\rho_e) \tag{13}$$

where $V_{c/a/e}$, $W_{c/a/e}$, and $\rho_{c/a/e}$ are the volume, weight, and density of cathode/anode/electrolyte, respectively. Because the weight of materials is determined by stored charge (Q) and specific capacity

$$W_{c/a/e} = Q/C_{c/a/e} \quad (14)$$

Equation (13) can be written as

$$E_d = [(C_c \times \rho_c)^{-1} + (C_a \times \rho_a)^{-1} + (C_e \times \rho_e)^{-1}]^{-1} \times V_{cell} \quad (15)$$

The compacted density of the electrode materials is used where possible: PbO_2 4.2 (ref. 55); Pb 4.35 (ref. 55); AC 0.7 (ref. 56); PTO 1.65; 4.4 M H_2SO_4 1.255; $LiMn_2O_4$ 2.8 (ref. 57); $LiCoO_2$ 4.0 (ref. 57); $LiTi_2(PO_4)_3$ 2.6 (ref. 58); polyimide 1.58; PPTO 1.68; $Ni(OH)_2$ 2.6 (refs 59,60); MmH 4.75 (ref. 60); PAQS 1.69; ZnO 2.25 (ref. 61); 10 M KOH 1.445. The theoretical density is used for CuHCF (1.8 (ref. 62)) because the compacted density is not found in the literature. The theoretical density of $Na_3V_2(PO_4)_2F_3$ (3.2 (ref. 63)) is used for $Na_3V_2(PO_4)_3$ because the lack of data for the latter. Specific power is the quotient of specific energy divided by the time it takes to discharge a cell completely. To demonstrate the potentially achievable specific energy in a cell configuration, several hypothetically plausible electrode materials are considered. 'PbO_2 (90%)' denotes PbO_2 with a utilization of 90% (ref. 64) instead of the typical ~50% in commercial Pb-acid batteries. 'Quinone†' refers to quinones with the specific capacity of PTO (395 mAh g^{-1}) and the reduction potential of anthraquinone (AQ) in acid (0.16 V versus SHE), $LiTi_2(PO_4)_3$ in neutral (−0.52 V versus SHE), and 200 mV lower than PAQS in alkaline (−0.80 V versus SHE). '$LiCoO_2$†' differs from the $LiCoO_2$ in Fig. 3 in that half a lithium is extracted from the latter (corresponding theoretically to 140 mAh g^{-1} and experimentally to 100 mAh g^{-1}) while more is extracted from the former (leading to ≥ 200 mAh g^{-1}). $LiCoO_2$† can only couple with quinone anodes because OER will inevitably occur towards the end of charge much like the situation for PbO_2 and $Ni(OH)_2$, and only quinones support the oxygen cycle among anodes for near-neutral conditions.

Cost analysis. Some of the chemicals used in the synthesis procedure reported herein were replaced with equivalents used in larger scales for a more realistic scaled-up cost estimation. PTO can be synthesized via either Ru- or Cr/Mn-based oxidation procedures[65–67]. The cost of PTO is calculated based on the cheaper Cr- (not even cheaper Mn-) based methods where pyrene ($1 kg^{-1}) is oxidized by 4 eq. of CrO_3 ($2 kg^{-1}) to afford the product in ~85–90% yields. The synthesis of PPTO considers the same procedure as reported herein except for replacing the reductant $SnCl_2$ and oxidant DDQ with Na_2S ($0.5 kg^{-1}) and $FeCl_3$ ($0.25 kg^{-1}), respectively, during the conversion of **2** to **3** (65–70% yield), and replacing DMAP with pyridine ($2.5 kg^{-1}) for the polymerization (80–85% yield). PAQS is synthesized by the reaction between equimolar 1,5-dichloroanthraquinone ($2 kg^{-1}) and Na_2S (80–85% yield). The cost of polyimide is calculated based on poly[*N*,*N*'-(ethane-1,2-diyl)-1,4,5,8-naphthalenetetracarboximide][21], which is synthesized by the reaction between equimolar 1,4,5,8-naphthalenetetracarboxylic dianhydride ($2 kg^{-1}) and ethylenediamine ($2 kg^{-1}) (80–85% yield). Miscellaneous costs such as waste disposal, personnel, analytics, transportation, and so on will add ~10–15% to the cost at a 500-kg scale (>1,000-kg scale could be even lower). The cost for PTO, PPTO, PAQS, and polyimide is thus estimated at $4–6, $10–15, $3–4, and $3–4 per kg, respectively. The price for existing anode materials is available from various sources: Pb ($2–3 kg^{-1}) (ref. 68), AC ($14–18 kg^{-1}) (ref. 69), $LiTi_2(PO_4)_3$ ($22–25 kg^{-1}) (ref. 70), MmH ($15–18 kg^{-1}) (ref. 71), and ZnO ($2–3 kg^{-1}) (ref. 68). A fixed price for commercially available cathode materials is used for battery cost estimation: PbO_2 ($2 kg) (ref. 68), $LiMn_2O_4$ ($7.4 kg^{-1}) (ref. 72), $Ni(OH)_2$ ($9 kg^{-1}) (ref. 71). The battery cost reported in $kWh^{-1} is calculated based on cathode and anode active materials.

Data availability. The data that support the findings of this study are available within the article and its Supplementary Information or from the authors, see author contributions for specific data sets.

References

51. Sun, D. *et al*. High-rate $LiTi_2(PO_4)_3$@N–C composite via bi-nitrogen sources doping. *ACS Appl. Mater. Interfaces* **7,** 28337–28345 (2015).
52. Gheytani, S. *et al*. Chromate conversion coated aluminium as a light-weight and corrosion-resistant current collector for aqueous lithium-ion batteries. *J. Mater. Chem. A* **4,** 395–399 (2016).
53. An, Q. *et al*. Nanoflake-assembled hierarchical $Na_3V_2(PO_4)_3$/C microflowers: superior Li storage performance and insertion/extraction mechanism. *Adv. Energy Mater.* **5,** 1401963 (2015).
54. Wessells, C. D., Huggins, R. A. & Cui, Y. Copper hexacyanoferrate battery electrodes with long cycle life and high power. *Nat. Commun.* **2,** 550 (2011).
55. Yuesheng, F., Dian, H. & Yifeng, F. A storage battery resistant to pressure and beneficial to environmental protection, which is suitable for being used in deep sea. China patent WO2002101868 A1 (2002).
56. Sevilla, M. & Mokaya, R. Energy storage applications of activated carbons: supercapacitors and hydrogen storage. *Energy Environ. Sci.* **7,** 1250–1280 (2014).
57. Guo, H.-j. *et al*. Preparation of manganese oxide with high density by decomposition of $MnCO_3$ and its application to synthesis of $LiMn_2O_4$. *J. Power Sources* **189,** 95–100 (2009).
58. Pinus, I. Y. *et al*. On cationic mobility in Nasicon phosphates $LiTi_2(PO_4)_3$ and $Li_{0.9}Ti_{1.9}Nb_{0.1}(PO_4)_3$. *Solid State Ion.* **212,** 112–116 (2012).
59. Vicente, F., Gregori, J., García-Jareño, J. J. & Giménez-Romero, D. Cyclic voltammetric generation and electrochemical quartz crystal microbalance characterization of passive layer of nickel in a weakly acid medium. *J. Solid State Electrochem.* **9,** 684–690 (2005).
60. Zhangyong, H., Ping, C. & Guofeng, M. Method for manufacturing ultra-high temperature long-service life nickel-hydrogen batteries. China patent CN104577224 A (2015).
61. Melnicki, L. S., Lazic, I. & Cipris, D. *Role of Additives in Minimizing Zinc Electrode Shape Change: The Effect of Lead on the Kinetics of Zn(II) Reduction in Concentrated Alkaline Media* (Office of Naval Research, 1985); http://go.nature.com/2seO7fv
62. Ware, M. Prussian Blue: Artists' Pigment and Chemists' Sponge. *J. Chem. Educ.* **85,** 612–620 (2008).
63. Dugas, R., Zhang, B., Rozier, P. & Tarascon, J. M. Optimization of Na-ion battery systems based on polyanionic or layered positive electrodes and carbon anodes. *J. Electrochem. Soc.* **163,** A867–A874 (2016).
64. Moncada, A., Piazza, S., Sunseri, C. & Inguanta, R. Recent improvements in PbO_2 nanowire electrodes for lead-acid battery. *J. Power Sources* **275,** 181–188 (2015).
65. Hu, J., Zhang, D. & Harris, F. W. Ruthenium(III) chloride catalyzed oxidation of pyrene and 2,7-disubstitued pyrenes: an efficient, one-step synthesis of pyrene-4,5-diones and pyrene-4,5,9,10-tetraones. *J. Org. Chem.* **70,** 707–708 (2005).
66. Kassaee, M. Z., Hattami, M. & Moradi, L. Benzyltrimethylammonium fluorochromate(VI): a novel, efficient and selective oxidant. *Acta Chim. Slov.* **51,** 743–750 (2004).
67. Yao, M. & Wang, X. Preparation of phenanthraquinone. *Chem. Reagents* **6,** 367–368 (1992).
68. fastmarkets.com (2016); https://www.fastmarkets.com/base-metals
69. Weinstein, L. & Dash, R. Supercapacitor carbons. Have exotic carbons failed? *Mater. Today* **16,** 356–357 (2013).
70. alibaba.com (2016); http://www.alibaba.com
71. Klein, M. G., Eskra, M., Plivelich, R. & Ralston, P. *Bipolar Nickel Metal Hydride Battery* (Electro Energy, 2002); http://haszstudios.com/electro/products/technicalpapers/BipolarNickel.pdf
72. Henriksen, G. L., Amine, K., Liu, J. & Nelson, P. A. *Materials Cost Evaluation Report for High-Power Li-ion HEV Batteries* (2002); http://www.ipd.anl.gov/anlpubs/2003/01/45346.pdf